

ORIGINAL ARTICLE

Bio-inspired micropatterned hydrogel to direct and deconstruct hierarchical processing of geometry-force signals by human mesenchymal stem cells during smooth muscle cell differentiation

Chor Yong Tay¹, Yun-Long Wu², Pingqiang Cai³, Nguan Soon Tan^{4,5}, Subbu S Venkatraman³, Xiaodong Chen³ and Lay Poh Tan³

Micropatterned biomaterial-based hydrogel platforms allow the recapitulation of *in vivo*-like microstructural and biochemical features that are critical physiological regulators of stem cell development. Herein, we report the use of muscle mimicking geometries patterned on polyacrylamide hydrogels as an effective strategy to induce smooth muscle cell (SMC) differentiation of human mesenchymal stem cells (hMSCs). hMSCs were systemically coerced to elongate with varying aspect ratios (AR) (that is, 1:1, 5:1, 10:1 and 15:1) at a fixed projection area of $\sim 7000 \mu\text{m}^2$. The results showed engineered cellular anisotropy with an intermediate AR 5:1 and AR 10:1, promoting the expression of alpha smooth muscle actin (α -SMA) and enhancement of contractile output. Further mechanistic studies indicated that a threshold cell traction force of $\sim 3.5 \mu\text{N}$ was required for SMC differentiation. Beyond the critical cytoskeleton tension, hMSCs respond to higher intracellular architectural cues such as the stress fiber (SF) alignment, SF subtype expression and diphosphorylated myosin regulatory light-chain activity to promote the expression and incorporation of α -SMA to the SF scaffold. These findings underscore the importance of exploiting biomimetic geometrical cues as an effective strategy to guide hMSC differentiation and are expected to guide the rational design of advanced tissue-engineered vascular grafts.

NPG Asia Materials (2015) 7, e199; doi:10.1038/am.2015.66; published online 10 July 2015

INTRODUCTION

Within the context of a multifarious extracellular matrix microenvironment, stem cells are presented with a wide spectrum of important biochemical, structural and mechanical regulatory stimuli.¹ Apart from the classical use of soluble biochemical factors to drive stem cell differentiation, there is accumulating evidence that biophysical alteration to the cell shape could potentially skew lineage commitment.^{2,3} However, our current understanding, especially on how local geometrical constraints may influence mesenchymal stem cell (MSC) differentiation along the smooth muscle lineage, remains incomplete.

Adult MSCs are a valuable cell source for regenerative medicine.^{4–6} Several reports have demonstrated that MSCs from various tissue origins are able to differentiate into smooth muscle cells (SMCs), a key component of the vasculature that lines the blood vessels, urinary tract and digestive tract.^{7–9} However, the key to unlocking MSCs' potential for vascular tissue engineering would require a

concerted multifactorial strategy to modulate the differentiation of MSCs into SMCs. Among the different strategies explored to control MSC differentiation, the use of biomaterialistic-driven cues such as matrix elasticity¹⁰, applied mechanical loading^{11,12} and even tailoring of cell shape^{13–15} have gained prominence in recent years. Arguably, the use of cell shape to steer stem cell lineage commitment is particularly attractive for regenerative medicine because organizational guidance can easily be incorporated as part of the biomaterial scaffold design to engineer stem cell adhesion patterns.

Although cell shape has long been acknowledged to have an essential role in cell physiology, it is unclear whether cell shape remodeling is a manifestation of the original capabilities of cells or cell shape actually pre-determines function. Using microcontact printing, researchers can independently manipulate cell shape and examine its role in the regulation of fundamental biological processes such as cell survival, proliferation and differentiation.¹⁵ In the context of SMC development, it has been shown that SMC elongation precedes the

¹Department of Chemical and Biomolecular Engineering, National University of Singapore, Singapore, Singapore; ²School of Pharmaceutical Science, Xiamen University, Xiamen, Fujian, China; ³School of Materials Science and Engineering, Nanyang Technological University, Singapore, Singapore; ⁴School of Biological Sciences, Nanyang Technological University, Singapore, Singapore and ⁵Institute of Molecular and Cell Biology, Singapore, Singapore

Correspondence: Dr CY Tay, Department of Chemical and Biomolecular Engineering National University of Singapore, 4 Engineering Drive 4, Singapore 117585, Singapore.

E-mail: chetcy@nus.edu.sg

or Associate Professor LP Tan, School of Materials Science and Engineering, Nanyang Technological University, N4.1, Nanyang Avenue, Singapore 639798, Singapore.

E-mail: lptan@ntu.edu.sg

Received 27 January 2015; revised 30 March 2015; accepted 27 April 2015

production of SMC-specific proteins.¹⁶ Conversely, the rounding of murine embryonic MSCs cultured on a multi-perforated polycarbonate surface represses the expression of SMC proteins.¹⁷ At the tissue level, aligned spindle-shaped SMCs is also important to impart functional mechanical strength during muscle contraction. Recently, it was demonstrated that the degree of cell spreading could potentially introduce a mechanical bias to the process of lineage commitment in MSCs. For instance, bone marrow-derived human mesenchymal stem cells (hMSCs) micropatterned on large fibronectin (FN) islands (10 000 μm^2) treated with transforming growth factor beta (TGF- β) promoted expression of SMC contractile markers such as alpha smooth muscle actin (α -SMA) and calponin, whereas hMSCs grown on small FN islands (1024 μm^2) favored chondrogenesis.¹⁴ Similarly, our previous works demonstrated that coerced cellular elongation of hMSCs on micropatterned poly (lactide-co-glycolide acid) thin film is an effective strategy to regulate the FAK-ERK signaling axis and mediate shape-dependent regulation of hMSC-lineage commitment, predominantly toward the muscle lineage in the absence of soluble factors.^{13,18} Collectively, these studies strongly suggest that cell shape is a potent regulator of hMSC differentiation.

Although an elongated morphology is intrinsic to the shape of contractile SMCs, a systematic study examining how different degrees of cell elongation could potentially affect SMC differentiation of MSCs has never been attempted. Inspired by the anisotropic muscle cell architecture, we examined the effect of hMSC elongation on the expression and subcellular localization of α -SMA, a key differentiation marker of SMCs. The attachment of the hMSCs was confined to discrete FN islands on the surface of a polyacrylamide (PAA) hydrogel, and cells were coerced to adopt shapes with aspect ratios (AR) ranging from 1:1 to 15:1 while keeping the cell-spreading area constant. Under the effect of TGF- β 1-induced SMC differentiation, it was observed that SMC-like geometries, such as AR 5:1 and 10:1, offered the optimal shape for expression and recruitment of the mechanosensitive protein α -SMA to the filamentous actin (F-actin) cytoskeletal scaffold. The shape-mediated effect was closely associated with the interdependency of the magnitude of the contractile force, spatial distribution of focal adhesions (FAs) and expression of distinct stress fiber (SF) subtypes. Based on our findings, we propose a model to describe the decision-making process undertaken by hMSCs during TGF- β 1-induced SMC differentiation in a geometry-force-dependent manner. We found that a threshold traction stress and proper architectural configuration are essential to promote α -SMA expression. Taken together, our findings provide critical leads into the interplay of cellular architecture and biochemical induction of SMC differentiation in hMSCs and are expected to yield useful guiding principles for the design and construction of advanced functional vascular tissue grafts.

MATERIALS AND METHODS

Preparation and characterization of the micropatterned compliant PAA hydrogel

In brief, glass coverslips (22 \times 22 mm) were first soaked in ethanol and flamed-dried to clean the surface of the glass. The coverslips were then salinized by soaking in 2% (v/v) 3-(trimethoxysilyl)propyl methacrylate (Sigma-Aldrich, St Louis, MO, USA) and 1% (v/v) glacial acetic acid in ethanol for \sim 10 min at room temperature. Next, the coverslips were removed and dried with purified nitrogen gas. PAA solution consisting of either 8% acrylamide and 0.48% bis-acrylamide or 4% acrylamide and 0.15% bis-acrylamide in ultrapure water was prepared and passed through a filter with a 0.22 μm pore size. To initiate cross-linking, tetramethylethylenediamine (1:1000) (Bio-Rad Laboratories, Hercules, CA, USA) and 10% ammonium persulfate (1:100) were added to the acrylamide and bis-acrylamide mixture and vortexed briefly for \sim 5 s. Immediately afterward, 35 μl of the mixture was pipetted onto a piece of clean

transparency sheet, and the coverslips were carefully placed onto the solution with the silanized surface facing down. The coverslips were allowed to stand for 20 min at room temperature to complete polymerization, and then the top coverslip with the attached PAA hydrogel was gently removed. The viscoelastic behavior of the prepared PAA hydrogels was characterized with an automated rotational rheometer (Physical MCR 501, Anton Paar, Graz, Austria) in ambient conditions. For this study, the PAA hydrogel with Young's modulus of 37.5 kPa and 1.6 kPa was used. The PAA-coated coverslips were stored in phosphate-buffered saline (PBS) at 4 $^{\circ}\text{C}$.

Next, 350 μl of 0.2 mg ml^{-1} of the heterobifunctional protein cross-linker sulfosuccinimidyl-6-(4-azido-2-nitrophenylamino)-hexanoate (Protechem, Loves Park, IL, USA) in 50 mM of 4-(2-hydroxyethyl)-1-piperazineethanesulfonic acid buffer (pH 8.5) was pipetted to the surface of the PAA hydrogel, and it was exposed to ultraviolet (UV) (365 nm) for \sim 15 min at room temperature. At the end of the reaction, the sulfosuccinimidyl-6-(4-azido-2-nitrophenylamino)-hexanoate became a rusty brown color. The PAA hydrogel-coated coverslips were then rinsed thoroughly three times with 50 mM of 4-(2-hydroxyethyl)-1-piperazineethanesulfonic acid buffer (pH 8.5) to remove the excess unbound sulfosuccinimidyl-6-(4-azido-2-nitrophenylamino)-hexanoate. After being dried at 60 $^{\circ}\text{C}$ for 20 min to dehydrate the gel, the samples were ready to be microprinted.

Poly dimethylsiloxane stamps bearing the desired micropatterns were prepared via a standard lithographic method, cleaned and stored as described previously.¹¹ With the micropatterned surface facing up, 50 $\mu\text{g ml}^{-1}$ of human plasma-derived FN (Gibco, Carlsbad, CA, USA) were added to the poly dimethylsiloxane stamp and allowed to stand for 1 h under sterile conditions. At the end of the 'inking' step, the excess FN was removed and the stamp was dried with nitrogen gas. Conformal contact of the FN 'inked' poly dimethylsiloxane stamp's micropatterned surface was then made with the previously prepared PAA hydrogel-coated coverslips for \sim 15 min under sterile conditions to transfer-print the FN patterns onto the substrate.

Cell culture and induction of SMC differentiation

Bone marrow-derived hMSCs (Lonza, Basel, Switzerland) were routinely expanded in MSC basal medium (Lonza) for optimal expansion and were subcultured at a density of 4000–6000 cells cm^{-2} . The medium was changed every 2–3 days. Low-glucose Dulbecco's Modified Eagle's Medium containing L-glutamine (Sigma) supplemented with 1% antimycotic antibiotic solution and either 10% or 1% fetal bovine serum (FBS Gold, PAA, Buckinghamshire, UK) were used as the standard growth medium for the experimental studies. Unless stated otherwise, growth medium containing 1% fetal bovine serum was used for the micropatterned cells. Only early-passage hMSCs (passages 4–6) were used in the experimental studies. The cells were maintained at 37 $^{\circ}\text{C}$ in a humidified atmosphere of 5% CO_2 . PBS (PAA) and 0.05% trypsin-ethylenediaminetetraacetic acid (Gibco) were used for washing and cell-detachment purposes, respectively. To induce smooth muscle differentiation, hMSCs were cultured overnight in standard growth medium. Then, the medium was replenished with fresh medium containing 10 ng ml^{-1} of TGF- β 1 (Peprotech, Rocky Hill, NJ, USA) for an additional 7 days before the samples were retrieved for further analysis.

Real-time-PCR

Real-time-PCR was used to ascertain differentiation of hMSCs along the SMC lineage under the influence of TGF- β 1 at the transcript level. Total RNA was harvested and purified using an RNeasy mini kit (Qiagen, Hilden, Germany) and reverse transcribed using the iScript cDNA synthesis kit (Bio-Rad Laboratories). Real-time-PCR was conducted on a CFX 96 real-time system (Bio-Rad Laboratories) using the SsoAdvanced SYBR Green supermix (Bio-Rad Laboratories) and the suggested cycling conditions provided by the manufacturer. Primer sequences of genes of interest are listed in Table 1.

Measurement of SF alignment orientation

High-resolution confocal microscopy images of the micropatterned cells counterstained with tetramethyl rhodamine iso-thiocyanate-phalloidin were used to examine the spatial arrangement and orientation of the SFs. All of the images were captured using identical camera acquisition parameters to enable

Table 1 Primers used for quantitative PCR

Gene ID	Genbank accession number	Description gene/protein	Sequence (5'–3')	Amplicon length (bp)
ACTB	NM_001101	β -actin	CATGTACGTTGCTATCCAGGC CTCCTTAATGTCACGCACGAT	250
ACTA2	NM_001613	α smooth muscle actin 2	CTATGAGGGCTATGCCTTGCC GCTCAGCAGTAGTAAC- GAAGGA	122
CNN1	NM_001299	Calponin 1	GAACGTGGGAGTGAAGTACGC CAGCCCAATGATGTTCCGC	85
SM22 α	NM_001001522	TAGLN	CCGTGGAGATCCCAACTGG CCATCTGAAGGCCAATGACAT	104

cross-comparisons. Stress fiber alignment was quantitatively assessed using the OrientationJ¹⁹ plugin on the ImageJ platform to construct the hue–saturation–brightness color-coded map that showed the orientation of localized SFs. Circular histograms that measure the distribution of the local SF angles were generated from 15 individually micropatterned cells for each shape.

Immunocytochemical staining

After the stipulated time of culture, the cells were washed gently three times in PBS and fixed with 4% paraformaldehyde for 15 min at room temperature, followed by three more washes in PBS. To permeabilize the fixed cells, the cells were further incubated with 0.2% of Triton X-100 in PBS for 10 min at room temperature. Next, the cells were blocked for non-specific binding of antibodies with 2% bovine serum albumin in PBS for 1 h at room temperature. For immunodetection of the targeted proteins, the primary antibodies were diluted in 0.2% bovine serum albumin in PBS containing 0.02% of Triton X-100 overnight at 4 °C. Subsequently, the cells were washed three times with PBS and counterstained with the respective secondary fluorescently tagged antibodies for 1 h in the dark at room temperature. The samples were then mounted using ProLong Gold antifade reagent with 4',6'-diamidino-2-phenylindol (Molecular Probes, Carlsbad, CA, USA) onto a microscope glass. Immunofluorescence images were visualized and captured using a Nikon 80i Eclipse upright fluorescent microscope or an Olympus FluoView FV1000 laser scanning confocal microscope (Olympus, Tokyo, Japan). The same camera acquisition settings were used for all of the samples for each experiment to ensure fair and representative analysis. Details of the antibodies, including the dilution factors used in this study, were as follows: rabbit polyclonal anti-FN (Sigma-Aldrich, 1:400); mouse monoclonal anti-vinculin (Millipore, Billerica, MA, USA) (1:400); rabbit polyclonal anti-smooth muscle actin (Abcam, Cambridge, UK) (1:100); mouse monoclonal anti-phospho-myosin light chain 2 (Ser19) (Cell Signaling Technology, Danvers, MA, USA) (1:200); rabbit polyclonal anti-phospho-myosin light chain 2 (Thr18/ Ser19) (Cell Signaling Technology, 1:200); Alexa Fluor 488 chicken anti-rabbit (Molecular Probes, 1:250); Alexa Fluor 488 chicken anti-mouse (Molecular Probes, 1:250); Alexa Fluor 594 chicken anti-rabbit (Molecular Probes, 1:250); and Alexa Fluor 594 chicken anti-mouse (Molecular Probes, 1:250). F-actin was counterstained with tetramethyl rhodamine iso-thiocyanate-conjugated phalloidin (Millipore, 1:400). Images used for comparisons of different cells or treatment regimens were acquired using the same instrument settings and exposure times and were processed similarly.

Image analysis

α -SMA fluorescence-intensity levels per cell were quantified by extracting the mean gray value using ImageJ software. Colocalization of α -SMA and F-actin was determined by computing the Mander's colocalization coefficient with the aid of the JACoP plugin installed in ImageJ.²⁰ The colocalization index measures the overlap of the α -SMA fluorescence signal with the F-actin fluorescence signal within the area of the micropatterned cells. Fifteen randomly chosen micropatterned cells from each shape group were chosen for each experiment.

Measurement of cell traction force

To measure the cell traction force (CTF), a monolayer of fluorescent beads embedded in the top layer of the PAA hydrogels was used as a substrate for the hMSC culture. In brief, 100 μ l of diluted yellow–green FluoSpheres microspheres (0.2 μ m, carboxylate-modified, 0.1 vol%, Molecular Probes) was cast onto the surface of glass coverslips, which were cleaned with oxygen plasma and further treated with 1H,1H,2H,2H-perfluorooctyltrichlorosilane to fabricate a monolayer of fluorescent beads on the coverslip. This fluorescently marked coverslip was applied to sandwich acrylamide and bis-acrylamide solution before polymerization with another amino-silanized coverslip as described above. To calculate CTFs, fluorescent bead displacements induced by hMSC traction and elastic moduli of PAA substrate were applied. Images of the fluorescent beads before and after cell trypsinization were used to track the spatial displacement of the beads as position markers, which were further translated into corresponding traction stress mapping in pseudocolor.²¹ The cell traction mapping indicated regions of traction stresses (dark blue to light pink, representing the range from low to high stress) and was based on the differential interference contrast image of hMSCs on the PAA substrate. In detail, calculation of the traction force \vec{f}_1 at discrete point (x_i, y_i) was based on the following formulation: $\vec{u}_t(x, y) = \sum_{i=1}^n G^{-1}(x - x_i, y - y_i) \vec{f}_i$, where G^{-1} denotes the Greens' tensor and \vec{u}_t denotes the fluorescent bead displacements. The total CTF (F) is an integral of the traction field magnitude over the whole cellular area, $F = \int \int \sqrt{T_x^2(x, y) + T_y^2(x, y)} dx dy$, where $T(x, y) = [T_x(x, y) + T_y(x, y)]$ is the continuous field of traction vectors located at typical spatial position (x, y) .

Statistical analysis

Statistical analysis was performed using Origin 9 (OriginLab, Northampton, MA, USA). Experimental data were subjected to Student's t -test or one-way analysis of variance where applicable. Fischer's least significant difference was used for pairwise comparisons. Details regarding the sample size and data analysis method pertaining to individual experiments are indicated in the associated text or figure legends.

RESULTS AND DISCUSSION

Engineering hMSC cytoskeletal anisotropy on bio-inspired hydrogel

To attain autonomous control over cell spreading, cell–cell interactions and cell elongation, discrete FN adhesive islands were micropatterned onto the PAA hydrogel using microcontact printing (Figure 1). Because it was previously shown that limiting hMSC spreading ~ 9.8 -fold could effectively divert SMC differentiation toward the chondrogenic lineage under the effect of TGF- β ,¹⁴ it is therefore imperative that we keep the cell-spreading area constant to delineate the confounding effects of cell spreading and SMC-differentiation events. Fidelity of the transferred printed FN protein (50 μ g ml⁻¹) on the gel surface was further validated via immunofluorescent staining. Arrays of the FN islands with uniform shapes and

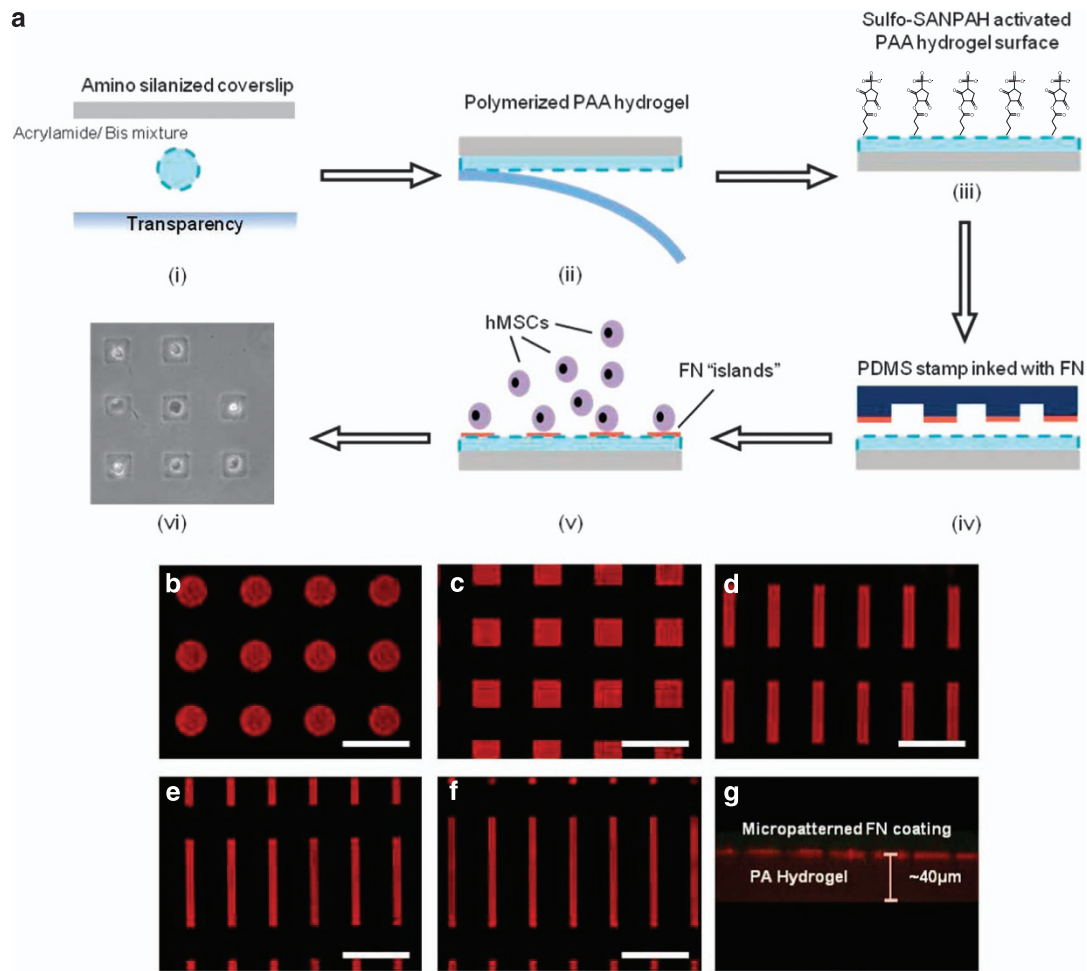


Figure 1 (a) Preparation and characterization of micropatterned polyacrylamide (PAA) hydrogel. To promote PAA hydrogel binding, coverslips were pretreated with APTES. (i) Thereafter, an acrylamide/bis mixture was sandwiched between the amino-silanized coverslips and a conventional transparency to ensure that the acrylamide and bis mixture was uniformly distributed on the coverslip. (ii) After the PAA hydrogel polymerized, the transparency was carefully peeled off to release the PAA hydrogel-coated coverslip. (iii) The PAA hydrogel surface was then covalently linked with sulfo-SANPAH to facilitate cross-linking of FN onto the surface. Thereafter, the PAA hydrogel was baked for a short time ~ 20 min at 60°C to ensure complete removal of water. (iv) FN protein with defined geometries was then transfer-printed using microcontact printing. (v) The PAA hydrogel was rehydrated with cell culture medium, followed by cell seeding. (vi) Geometrically defined cells could be validated using phase contrast microscopy. Representative immunolabeled FN islands consisting of (b) circular, AR (c) 1:1, (d) 5:1, (e) 10:1 and (f) 15:1 micropatterns on engineered PAA hydrogel. Scale bar, $200\ \mu\text{m}$. (g) Reconstructed Z stack image of micropatterned PAA hydrogel revealed the typical thickness of PAA hydrogel used for this study.

sizes could be attained using our micropatterned PAA hydrogel (Figures 1b–f). The patterns were deliberately designed to stretch the hMSCs with ARs ranging from non-anisotropic stretching such as a circle (Figure 1a) and AR 1:1 (Figure 1b) to geometries with varying anisotropy such as ARs 5:1 (Figure 1c), 10:1 (Figure 1d) and 15:1 (Figure 1e). High-resolution confocal images revealed that the thickness of the gel was $\sim 40\ \mu\text{m}$ (Figure 1g). Every individual FN island had a constant cell coverage area at $\sim 7000\ \mu\text{m}^2$, which was previously determined to be the average spreading area of the unpatterned hMSCs on conventional tissue cultured polystyrene plate surfaces. The cells were able to spread and fill up the entire FN island as early as 2 h post cell seeding.

Against a non-biofouling PAA hydrogel surface, the spatial localization and degree of cell spreading on the engineered substrate are determined solely by the patterned FN adhesive island. The cells were cultured on the substrate over an extended period (5 days) to ensure

that dynamic equilibrium of cell-spreading and cytoskeletal remodeling had been attained. Thereafter, the SF cytoskeleton was fluorescently labeled with tetramethyl rhodamine iso-thiocyanate and analyzed using the OrientationJ plugin¹⁹ to compute the orientation angles of the SFs. The color-coded hue-saturation-brightness maps corresponded to the localized SF orientation (Figures 2a–e). hMSCs adopting the circular and AR 1:1 geometries did not display a large-scale alignment of the SFs along the long axis of the cell body (Figures 2a and b), and there was a wide distribution of the average local SF orientation, as indicated by the circular histograms (Figures 2f and g). By contrast, increasing the AR promoted large-scale alignment of the SFs parallel to the longitudinal axis of the cell body (Figures 2c–e and h–j). These results concurred with those of previous studies^{18,22} and reinforced the notion that cells are able to respond to subtle geometrical cues by remodeling the cytoskeletal architecture.

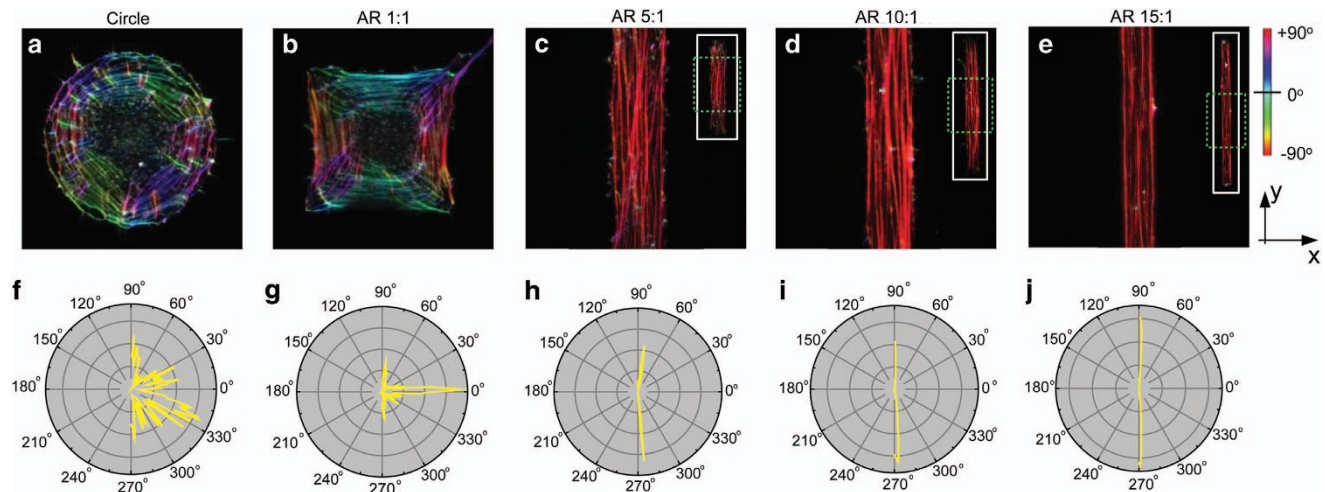


Figure 2 hMSC cell shape governs the spatial distribution and orientation of the SFs. The composite images, consisting of the filamentosous actin network (gray scale) superimposed with the hue–saturation–brightness (HSB) color-coded map of the SFs orientation for the (a) circle, (b) AR 1:1, (c) AR 5:1, (d) AR 10:1 and (e) AR 15:1 shaped cells in relation to the x axis. Scale bar = 15 μm . (f–j) Corresponding average circular histograms of the local SF orientation for the micropatterned cells. Numerical values denote the mean orientation angle of SFs from 15 individually patterned cells from each experimental group.

Cellular anisotropy and TGF- β 1 induction promoted the SMC phenotype of hMSCs

We next examined how cellular elongation that mimics *in vivo* SMC morphology and alignment of the SFs could potentially impact the expression and distribution of α -SMA. TGF- β 1 treatment clarified the synergistic role between biochemical factors and cell shape in SMC differentiation of hMSCs. TGF- β 1 is a potent stimulus capable of inducing SMC differentiation via activation of the TGF- β -SMAD signaling cascade in numerous adult tissue-derived MSCs.^{8,23} As expected, several key SMC-specific gene expressions such as ACTA2, SM22 α and CNN1 were significantly upregulated in hMSCs with increasing TGF- β 1 (10 ng ml⁻¹) treatment times (Supplementary Figure 1a–c). Among the SMC markers, ACTA2, which encodes α -SMA, displayed the highest expression level (approximately eightfold) after 7 days of culture. α -SMA is a major component of the contractile apparatus in skeletal muscle cells and its expression is a key milestone in SMC differentiation.¹⁴ Furthermore, the knockdown of α -SMA using RNA interference hampered cardiac differentiation of embryonic stem cells²⁴ and α -SMA null mice displayed impaired vascular contractility, tone and blood flow.²⁵ Successful TGF- β 1 treatment promoted incorporation of α -SMA into the actin-based SFs (Supplementary Figure 1d), which could augment the contractile force that is necessary to further drive the downstream events of SMC differentiation. Therefore, *de novo* expression and association of α -SMA to the SF cytoskeleton not only are important molecular events that mark the onset of SMC differentiation but also have a crucial role in vasculature development.

Strikingly, when the cells were treated with TGF- β 1 (10 ng ml⁻¹), there was a robust increase in α -SMA expression levels and association of α -SMA to the SFs with increasing cellular anisotropy (Figure 3a, Supplementary Figure S2a and b). In particular, rectangular cells with AR of 5:1 and AR 10:1 were observed to display higher mean α -SMA expression levels (approximately three- to fivefold) as compared with the circular and AR 1:1 cells (Figure 3b). However, this trend did not persist when the cells were stretched to a more extreme AR 15:1 (Supplementary Figure S2c), as reflected by a marked drop in α -SMA expression, which is comparable to the circular and AR 1:1 cells

(Figure 3b). Similarly, the incorporation of α -SMA to SF was highest in cells that adopted the AR 5:1 and AR 10:1 shapes (Figure 3c). Collectively, these observations suggest that controlled cellular anisotropy can promote the expression and recruitment of α -SMA to the actin SFs in the presence of TGF- β 1. However, excessive stretching of the cells became detrimental to SMC differentiation of hMSCs.

Expression and proper distribution of α -SMA are regulated by cellular anisotropy and optimal basal contractile output

The recent string of studies implicating altered contractile forces as a potential driving force to modulate stem cell lineage commitment may offer a plausible explanation for the observed shape-driven phenomenon. For instance, increased cell spreading was shown to enhance cell contractility by engaging the RhoA signaling cascade to promote bone differentiation.²⁶ By contrast, decreasing cell contractile forces by reducing AR¹⁵ or growing cells on a compliant surface²⁷ favored adipogenesis of hMSCs. Cell contractility is driven primarily by the actomyosin interaction and can be quantified using CTF microscopy.^{21,28,29} To investigate how cell shape influences CTF generation, the magnitude of traction stress was summed over the entire cell area. Figure 4a shows the representative color-coded heat traction stress map for the patterned cells with and without TGF- β 1 treatment. The cells exhibited spatially defined exertion of traction force vectors in response to the surface geometrical cue. Whereas cell traction was detected predominantly around the perimeter of the cells patterned on the circular FN Island, traction was the highest at the four corners of the AR 1:1 shaped cells. By contrast, traction was found to be concentrated at the apical ends of the elongated cells. In the absence of TGF- β 1, significantly higher basal CTF values were measured for the circular (6.1 \pm 0.4 μN) and AR 1:1 (5.4 \pm 0.4 μN)-shaped cells, whereas a marked decrease in CTF was observed with increasing AR (Figure 4b). Cells with AR 5:1, 10:1 and 15:1 registered an average CTF of 3.5 \pm 0.3 μN , 3.6 \pm 0.4 μN and 2.8 \pm 0.3 μN , respectively. Similarly, a reduction in CTF with increasing cell AR was recently reported by others; this may be attributable to an overall decrease in FA areas where the cells exert the tugging force on the underlying substrate.²² Furthermore, increasing cellular traction

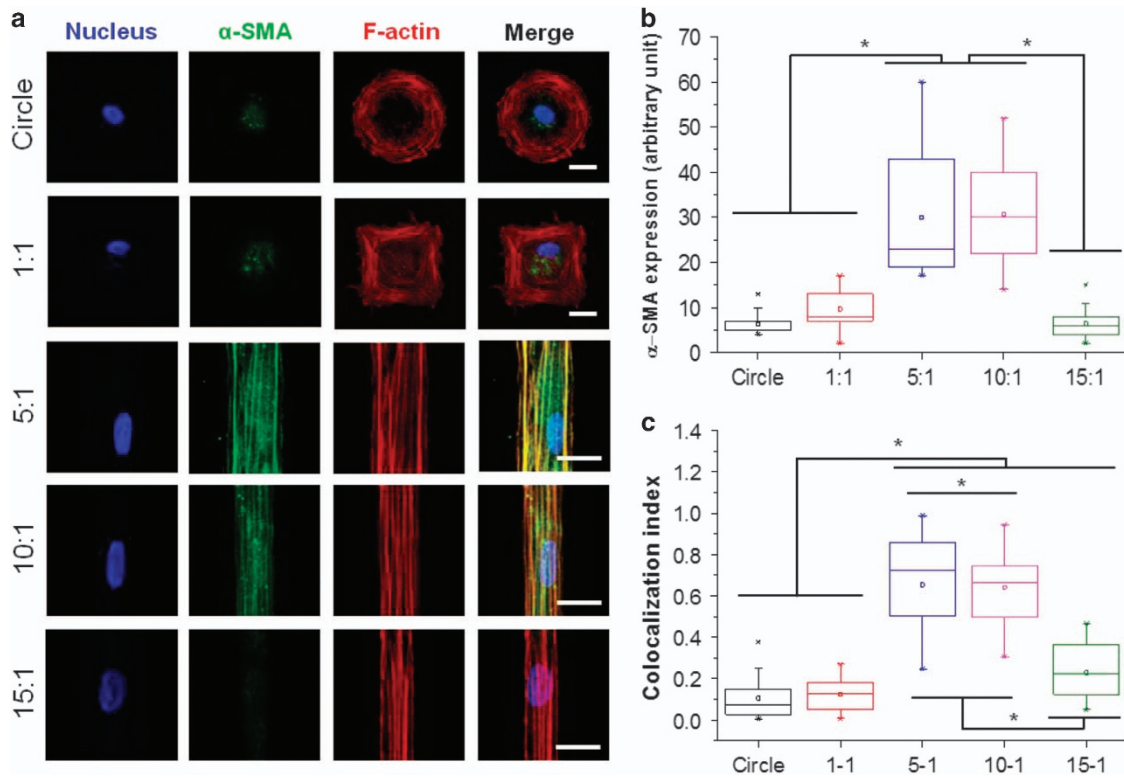


Figure 3 Cellular anisotropy promotes the expression and incorporation of α -SMA protein to stress fibers. **(a)** Representative immunofluorescence images of the micropatterned cells co-stained for α -SMA (green), F-actin (red) and cell nucleus (blue). Scale bar = 25 μ m. Box-whisker plots showing the mean values of **(b)** α -SMA expression level and **(c)** colocalization of the α -SMA and F-actin fluorescence signals. Data represents mean \pm s.d. derived from 15 individually patterned cells from each experimental group. * denotes significant difference between the compared experimental groups by analysis of variance followed by least significant difference *post hoc* test. ($P < 0.05$).

polarity (ratio between force along the principal axis in blue pseudocolor and the force detected along the green that is perpendicular to the principal one) was observed with increasing AR, indicating that cell shape serves as a key mediator in the regulation of structural organization and force orientation of hMSCs in determining their biomechanical polarity to the anisotropic patterns. After 7 days of culture in TGF- β 1-containing medium, all of the micropatterned cells exhibited a marginal increase in the average CTF compared with the untreated controls. Among the shapes examined, only cells with an AR of 5:1 or 10:1 exhibited a statistically significant increase in relative contractile force output between the TGF- β 1-treated and untreated cells by ~ 20 –30%. This observation, coupled with the notably higher expression of α -SMA for the AR 5:1 and AR 10:1 shapes (Figure 2), is consistent with previous reports that showed TGF- β treatment could promote cellular contractility owing to the enhanced expression of α -SMA contractile protein.^{30–32}

Because the basal CTF of the AR 15:1 cells is much lower than that of the AR 5:1 and 10:1 cells, we hypothesized that a threshold traction stress may be required to ensure proper α -SMA expression and re-localization of the actin fibers on activation of the TGF- β 1 signaling cascade. To explore this possibility, the intracellular contractile force of cells with pro-SMC differentiation shapes (that is, AR 5:1 and AR 10:1) was perturbed using mechanical and biochemical means (Supplementary Figures S3 and S4). Culturing the patterned cells on a softer PAA hydrogel (1.6 kPa) allowed us to mechanically relieve the intracellular tension while keeping the cell area and shape constant. The ‘soft’ gel corresponded to a 23-fold decrease in matrix stiffness as

compared with the gels used in the preceding sections. Interestingly, although cells on the softer gel displayed well-aligned F-actin architecture, α -SMA incorporation to the SFs was lacking (Figure 4c). Consistent with our finding, a recent study similarly reported a sharp decrease in α -SMA assembly into the SFs for hMSCs that were grown on soft (1 kPa) PAA hydrogel.⁹ With our engineered substrate, we were able to further conclude that the role of matrix stiffness dominates the effects of cell shape-dependent recruitment of α -SMA to the SFs framework. By contrast, when the cells were treated with cytoD (0.05 μ M), an actin-disrupting drug, and Y-27632 (2.5 μ M), a potent ROCK kinase inhibitor that interferes with myosin II driven contractility, expression of both the SFs and α -SMA was abolished (Figure 4c). Compared with the α -SMA expression in TGF- β 1-treated cells, we observed a significant decrease in α -SMA expression under the action of both contractile antagonists by ~ 10 -fold, whereas α -SMA expression was decreased by approximately twofold for cells cultured on the softer substrate (Figure 4d). Collectively, our results support the notion that a minimal traction force must be attained before the α -SMA can be recruited to the SFs. This may explain why excessive stretching of the MSCs body that is associated with a low basal level of CTF is not conducive for SMC differentiation.

Intermediate cell anisotropy promoted diphosphorylation state of the myosin regulatory light chain

Next, we asked why isotropic shapes, such as circle and AR 1:1, although generating high levels of CTF, did not support the expression and assembly of α -SMA into the SFs. Prompted by our earlier results,

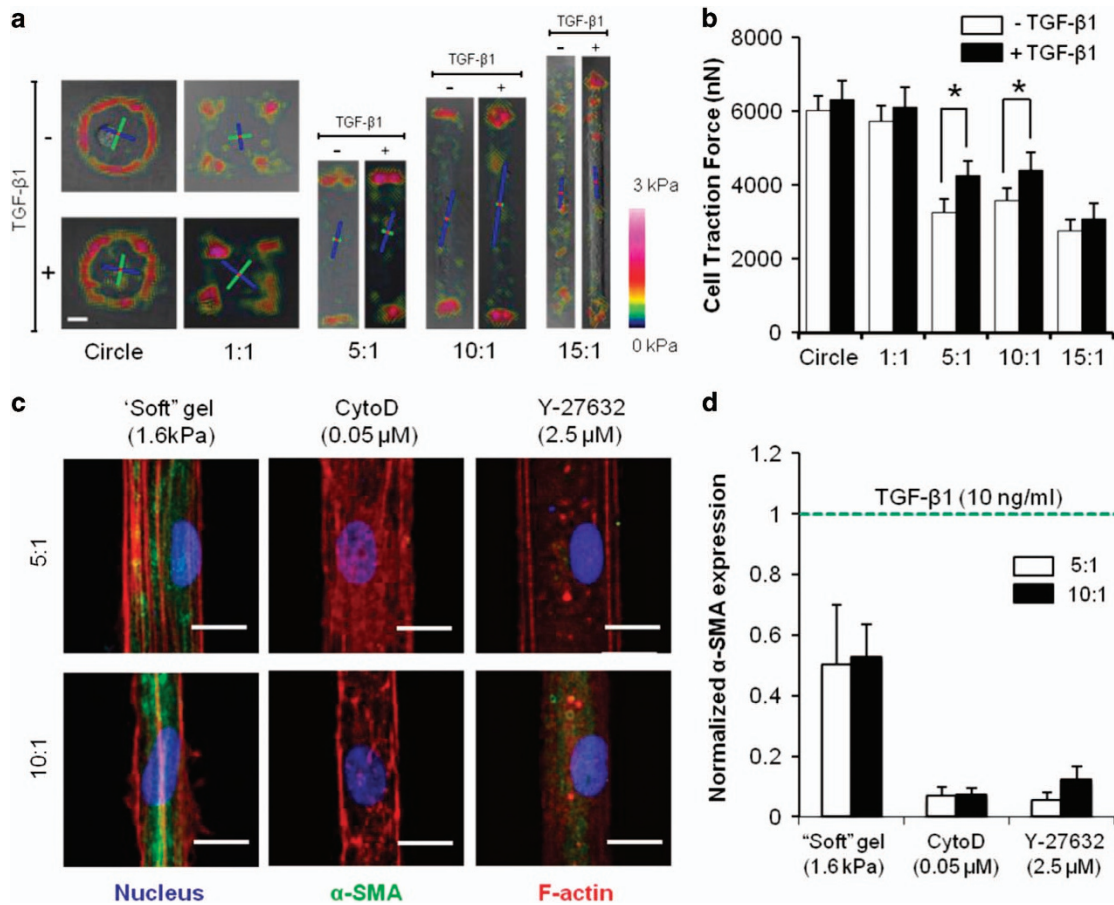


Figure 4 Cell shape governs contractile output of hMSCs. (a) Heat-scale traction stress map depicting the magnitudes of the cell-ECM tugging force of the micropatterned cells. (b) Computed average cell traction force as a function of cell shape. Data represent mean \pm s.d. derived from three independent samples for each hMSC-shape permutation. (c) Fluorescent images of the AR 5:1 and AR 10:1 cells labeled for α -SMA (green), F-actin (red) and cell nucleus (blue). (d) Normalized α -SMA expression level of the cells with different shape-treatment conditions. Data represents mean \pm s.d. derived from 15 individually patterned cells from each experimental group. *denotes significant difference with the untreated control by Student's *t*-test ($P < 0.05$). Scale bar = 25 μ m.

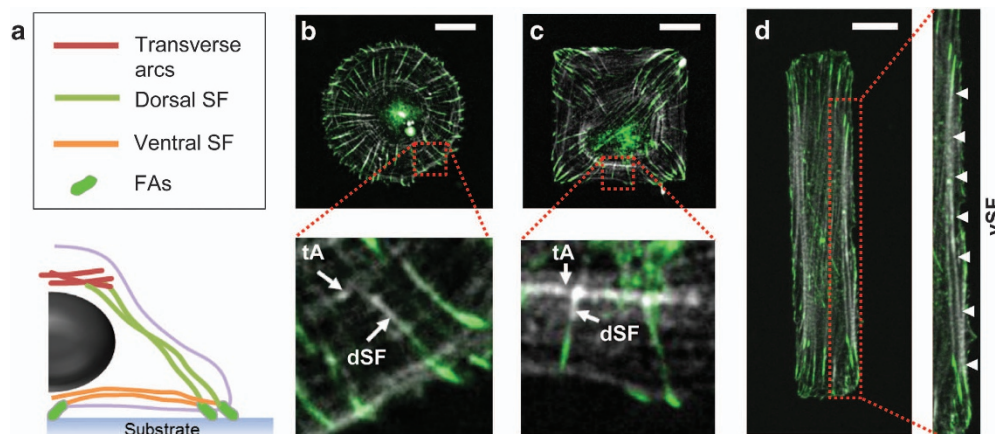


Figure 5 Micropatterned cells respond to geometrical cues by forming different types of SFs. (a) Illustration portraying the different classifications of SFs defined by their intracellular spatial distribution and interaction with FAs. Representative fluorescence images of the patterned cells counter stained for the actin cytoskeleton (gray) and vinculin (green), a major FA protein, for the (b) circular, (c) AR 1:1 and (d) rectangular (AR 5:1) cells acquired 5 days post cell seeding. The corresponding blown up images of regions of interest (red dashed box) clearly show the exclusive occurrence of tSF and dSF in the cells with circle and AR 1:1 shapes, whereas expression of vSF dominates the rectangular cells. Images were captured using the Nikon upright epifluorescence microscope with identical settings and exposure duration. Scale bar = 25 μ m.

we postulated that once the traction stress threshold has been attained, the cells may rely on higher-ordered architectural cues in determining the outcome. The F-actin cytoskeleton and FA assemblies represent a highly organized, self-regulated structural system to maintain mechano-stasis and cell shape. Recently, it was shown that the expression of large 'supermature' FAs could enhance cellular contractile forces and promote incorporation of α -SMA to SFs.³² Therefore, the differences in spatial distribution, size and density of FAs as a

function of cell shape may offer molecular insights into the observed shape-governed SMC differentiation of hMSCs.

Supplementary Figure S5a shows the fluorescent images of the micropatterned cells immunostained for vinculin, a mechanosensitive FA-associated protein. In general, the FAs were distributed around the periphery of the circular cells, whereas FAs accumulate at the corners of the square for cells with AR 1:1. By contrast, cells with AR 5:1 and AR 10:1 have FAs that are centrally located with preferential

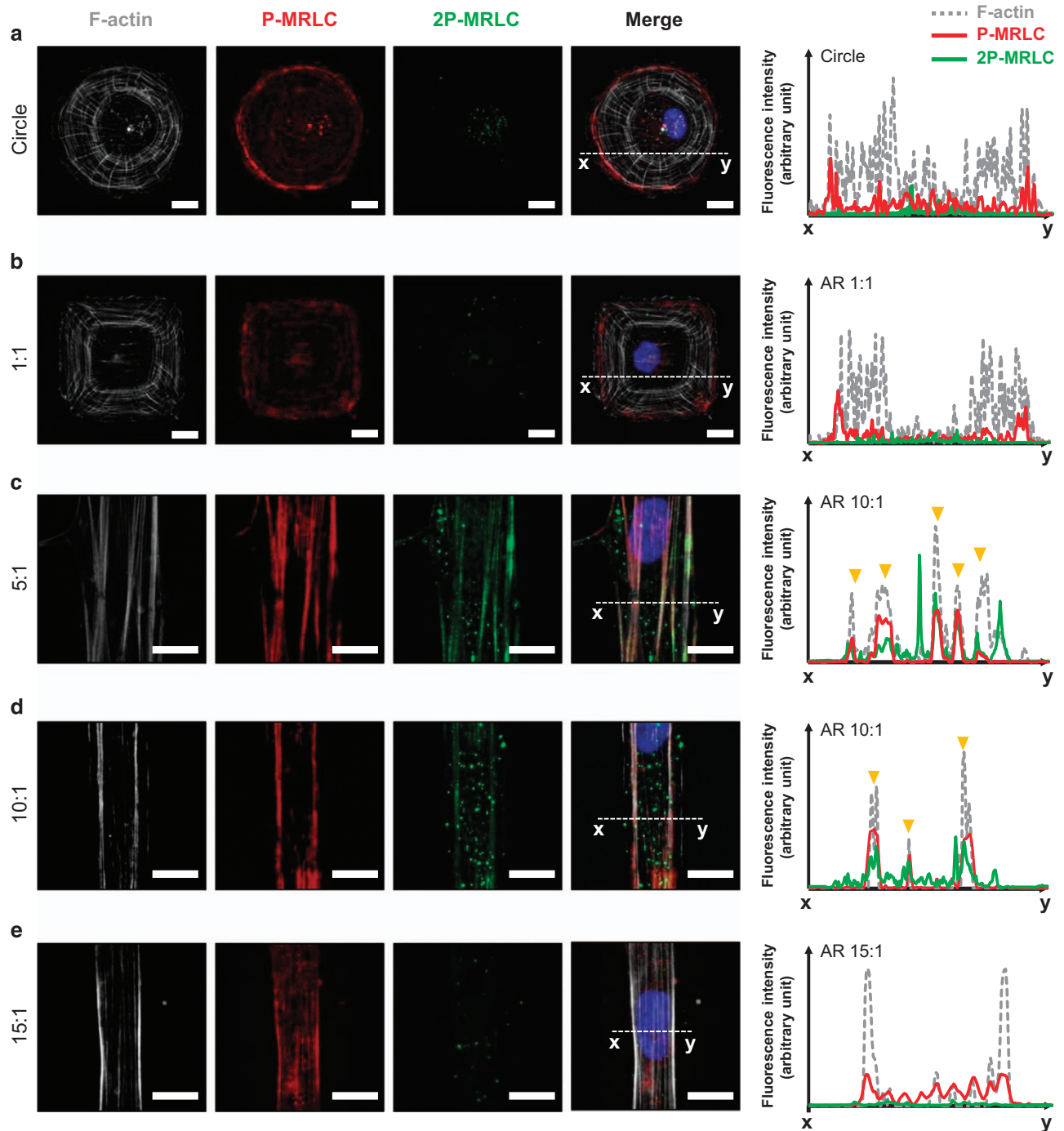


Figure 6 Phosphorylation of MRLC is cell shape-dependent and specific to SF subtypes. hMSCs patterned as (a) circle, (b) 1:1, (c) 5:1, (d) 10:1 and (e) 15:1 were fixed and co-stained for F-actin (gray), P-MRLC (red) and 2P-MRLC (green). Scale bar = 10 μ m. Right panel: Fluorescence-intensity profile graphs of F-actin, P-MRLC and 2P-MRLC across the x - y lines. Yellow arrows denote triple colocalization of all of the cytoskeletal proteins.

localization at the ends of the cells. Interestingly, for cells with AR 15:1, the FAs were sporadically distributed throughout the cell body. This finding suggests that as the cell body is stretched beyond a threshold AR, the cells may redistribute the anchor points across the entire cell body to maintain mechano-stasis within the all-encompassing confines of the FN islands. Next, the number of classical FAs ($1\text{--}5\ \mu\text{m}^2$) and supermature FAs ($> 5\ \mu\text{m}^2$) were profiled and compared for the micropatterned hMSCs as a function of cellular anisotropy (Supplementary Figure S5b). Interestingly, we did not observe any significant difference in terms of the number of expressed classical FAs and ‘supermature’ FAs among the cells with different shapes. The mean number of classical FAs in each group differed considerably within the range of $\sim 75\text{--}140$ per cell with high statistical variability, whereas the number of ‘supermature’ FAs per cell was ~ 50 regardless of the shape the cell assumed. Therefore, a simple correlation between cell shape, FA size and α -SMA expression cannot be established in our micropatterned system.

We next turned our attention to the organization of the SFs. Broadly speaking, SFs can be categorized into three subtypes—transverse arcs (tA), dorsal SFs (dSF) and ventral SFs (vSF)—based on their intracellular location and their interaction with FAs.³³ The definitions of the different classes of SFs are succinctly illustrated in Figure 5a. tAs are actin filament bundles that are typically oriented parallel to the advancing front of migrating cells and contract continuously during retrograde flow.^{33,34} tAs are not directly attached to FAs; instead, they are coupled to the dSFs to transmit tensile information to the extracellular matrix.³⁴ Conceptually, dSFs can be pictured as having one of their ends linked to a tA and the other to the FAs complex. dSFs are widely believed to be non-contractile because to the absence of periodic α -actinin–myosin distribution and the lack of contraction activity.³⁵ Conversely, a vSF is a highly contractile apparatus that is connected to the FAs at both ends and has an important role in cell adhesion and force generation.³⁴ Each SF subtype thus carries different contractile and structural signatures and may reflect a diverse ‘load-bearing’ capability.

Figure 5 shows the fluorescent composite images of the geometrically defined hMSCs that were co-stained for actin SFs (gray) and vinculin (green). For the cells that were coerced to adopt the circle

(Figure 5b) and AR 1:1 (Figure 5c) shapes, expression of the tAs and dSFs was readily detectable. Specifically, occurrence of the tAs was most prominent running parallel along the geometrical boundaries. The presence of tAs was accompanied by the occurrence of dSFs arranged at an angle to the tAs. In stark contrast, only vSFs were observed for the rectangular cells (Figure 5d). The vast dissimilarities in the types of SFs, as well as the actin network organization expressed in the cells with different shapes, hinted strongly that hMSCs might leverage on these cytoskeletal structural cues to mechanically influence the SMC differentiation process.

If the global architecture of the actin cytoskeleton governed by cell shape indeed regulates the process of α -SMA incorporation to the SFs, it has to be translated to differences in the contractile activities that are borne by the F-actin cables. One possible molecular target is the non-muscle myosin II that belongs to the superfamily of motor proteins. Non-muscle myosin II, which has an essential role in the generation of tension on actin filaments, is typically colocalized with the SFs.³⁶ Non-muscle myosin II is composed of three pairs of peptides: two heavy chains (230 kDa), two 170 kDa essential light chains and two regulatory light chains (RLCs). The contractile function of myosin is mediated by phosphorylation of the myosin RLCs (MRLCs).³⁷ Under the effect of myosin light-chain kinase, RLCs are phosphorylated at serine 19 (monophosphorylated; P-MRLCs). By contrast, diphosphorylation (2P-MRLCs) of RLCs at threonine 18 and serine 19 can be considered a relatively rare event that is typically detected in cells with enhanced cellular contractile force and stable myosin II filaments.³⁸ To examine how cell shape can impact the level and distribution of phosphorylated MRLCs, cells were triple-stained for the SFs, P-MRLCs and 2P-MRLCs using specific antibodies (Figure 6). Merged immunofluorescence images of the micropatterned cells revealed shape-dependent distribution and expression of both P-MRLCs and 2P-MRLCs. All micropatterned cells displayed P-MRLC-positive SFs, indicating that monophosphorylation of MRLCs is ubiquitous to the three SFs subtypes and that the cells are indeed under tension. Notably, staining of P-MRLC appears to be more intense near the cell boundaries with isotropic geometries (that is, circle and AR 1:1) (Figures 6a and b), suggesting a non-uniform distribution of intracellular contractility. By contrast, immunoreactivity of 2P-

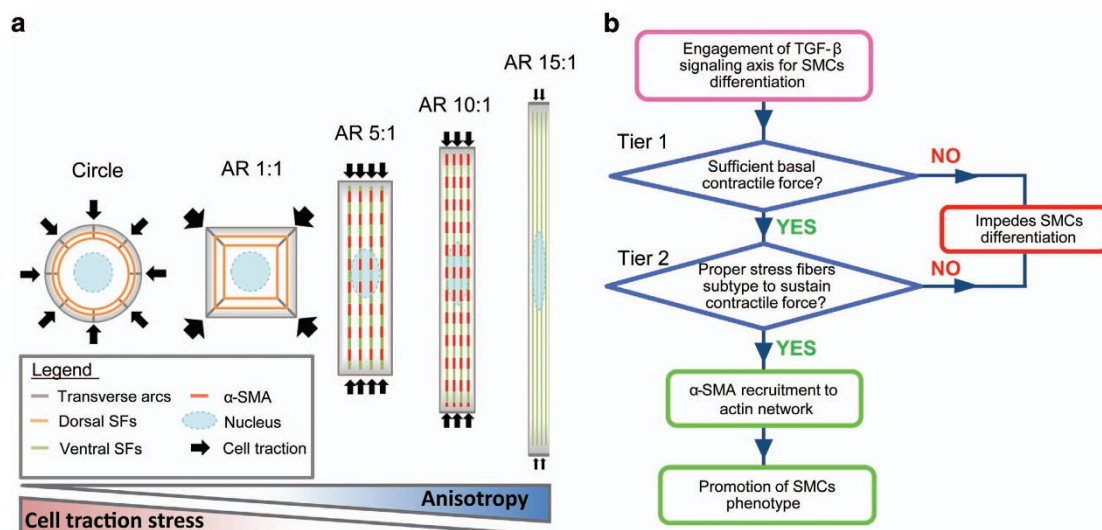


Figure 7 (a) Schematic to illustrate the complex inter-relationship between cell anisotropy-force generation-SF arrangements in determining the optimal degree of hMSC elongation for SMC differentiation. (b) Proposed cellular decision-making model to aid in the understanding of how hMSCs process and inter-regulate hierarchical structural cues to adopt an SMC phenotype under the influence of TGF- β 1.

MRLCs seems to be restricted to the elongated cells with AR 5:1 (Figure 6c) and 10:1 (Figure 6d), displaying the vSFs. This became apparent when the raw fluorescence intensity for each of the cytoskeletal protein targets was plotted across the x - y line. We observed colocalization of both the 2-MRLC and 2P-MRLC along the F-actin SFs (yellow arrows). We did not observe any 2P-MRLC staining for the cells with AR 15:1 (Figure 6e). The fact that diphosphorylation of MRLCs has been closely associated with enhancement of SF tension³⁸ lends further support that excessive stretching of cells diminishes the ability of the cells to generate and sustain sufficient contractile force for the recruitment of α -SMA to the SFs. Along the same vein, the concomitant absence of 2P-MRLC and α -SMA staining in the circle and AR 1:1 cells suggests that, once a critical threshold traction stress has been established, the formation of the right SF subtypes (that is, vSFs) is an important co-requisite for SMC differentiation of hMSCs.

CONCLUSION

In summary, using a bio-inspired micropatterned hydrogel platform, the shape-dependent SMC differentiation of hMSCs under the effect of TGF- β 1 was examined. By keeping the cell-spreading area constant while varying cell anisotropy, we were able to systematically examine the synergy between stem cell shape and biological signals. It was shown that controlled cellular anisotropy has a significant role in governing the expression and subcellular distribution of α -SMA protein, a finding that is of high relevance to vascular tissue engineering. The optimal shape (AR 5:1 and 10:1) for proper recruitment of α -SMA to the existing SFs corresponded to the generation of intermediate contractile force with appropriate cytoskeletal architecture that can help support and sustain long-range actomyosin tension (Figure 7a). To conceptually unify all of these findings, we propose a two-tiered scheme depicting how global cytoskeletal arrangement, contractile force and FA distribution collectively affect SMC differentiation of hMSCs (Figure 7b). There are two critical decision-making junctures faced by hMSCs that will determine whether the shape is favorable for SMC differentiation. The first deciding factor (tier 1) is denoted by the need to establish a critical level of traction force, followed by the cytoskeletal arrangement (tier 2) that will govern the expression of SF subtypes and ability to sustain and positively drive intracellular tension. Such complex interdependent regulation of cell shape, F-actin cytoskeleton, FA assembly and contractile force generation not only sheds valuable insights into how hMSCs could process these confounding biomechanical signals in a hierarchical manner but may also serve as a useful model to explain why SF alignment along the longitudinal axis of the cells is most conducive for contractile functionality in vascular SMCs. Taken together, our findings revealed that precise control over cellular elongation is a viable strategy that could be exploited to produce exogenous SMC-based tissue grafts.

CONFLICT OF INTEREST

The authors declare no conflict of interest.

ACKNOWLEDGEMENTS

The authors gratefully acknowledge financial support from the Ministry of Education Academic Research Grants (R-279-000-376-112 to CYT) and Nanyang Technological University Tier 1 grant (RGT24/13). CYT thankfully acknowledges support from the Lee Kuan Yew Postdoctoral Fellowship.

- Lane, S. W., Williams, D. A. & Watt, F. M. Modulating the stem cell niche for tissue regeneration. *Nat. Biotechnol.* **32**, 795–803 (2014).
- Guilak, F., Cohen, D. M., Estes, B. T., Gimble, J. M., Lietke, W. & Chen, C. S. Control of stem cell fate by physical interactions with the extracellular matrix. *Cell Stem Cell* **5**, 17–26 (2009).
- Tay, C. Y., Koh, C. G., Tan, N. S., Leong, D. T. & Tan, L. P. Mechanoregulation of stem cell fate via micro/nano-scale manipulation for regenerative medicine. *Nanomedicine (Lond)* **8**, 623–638 (2013).
- Harris, L. J., Abdollahi, H., Zhang, P., McIlhenny, S., Tulenko, T. N. & DiMuzio, P. J. Differentiation of adult stem cells into smooth muscle for vascular tissue engineering. *J. Surg. Res.* **168**, 306–314 (2011).
- Leong, D. T., Khor, W. M., Chew, F. T., Lim, T. C. & Huttmacher, D. W. Characterization of osteogenically induced adipose tissue-derived precursor cells in 2-dimensional and 3-dimensional environments. *Cells Tissues Organs* **182**, 1–11 (2006).
- Leong, D. T., Nah, W. K., Gupta, A., Huttmacher, D. W. & Woodruff, M. A. The osteogenic differentiation of adipose tissue-derived precursor cells in a 3D scaffold/matrix environment. *Curr. Drug Discov. Technol.* **5**, 319–327 (2008).
- Williams, C., Xie, A. W., Ermani, S., Yamato, M., Okano, T., Ermani, S. M. & Wong, J. Y. A comparison of human smooth muscle and mesenchymal stem cells as potential cell sources for tissue-engineered vascular patches. *Tissue Eng. Part A* **18**, 986–998 (2012).
- Chen, S. & Lechleider, R. J. Transforming growth factor-beta-induced differentiation of smooth muscle from a neural crest stem cell line. *Circ. Res.* **94**, 1195–1202 (2004).
- Park, J. S., Chu, J. S., Tsou, A. D., Diop, R., Tang, Z., Wang, A. & Li, S. The effect of matrix stiffness on the differentiation of mesenchymal stem cells in response to TGF-beta. *Biomaterials* **32**, 3921–3930 (2011).
- Engler, A. J., Sen, S., Sweeney, H. L. & Discher, D. E. Matrix elasticity directs stem cell lineage specification. *Cell* **126**, 677–689 (2006).
- Kurpinski, K., Chu, J., Hashi, C. & Li, S. Anisotropic mechanosensing by mesenchymal stem cells. *Proc. Natl Acad. Sci. USA* **103**, 16095–16100 (2006).
- Leong, W. S., Wu, S. C., Pal, M., Tay, C. Y., Yu, H., Li, H. & Tan, L. P. Cyclic tensile loading regulates human mesenchymal stem cell differentiation into neuron-like phenotype. *J. Tissue Eng. Regener. Med.* **6**, s68–s79 (2012).
- Tay, C. Y., Yu, H., Pal, M., Leong, W. S., Tan, N. S., Ng, K. W., Leong, D. T. & Tan, L. P. Micropatterned matrix directs differentiation of human mesenchymal stem cells towards myocardial lineage. *Exp. Cell Res.* **316**, 1159–1168 (2010).
- Gao, L., McBeath, R. & Chen, C. S. Stem cell shape regulates a chondrogenic versus myogenic fate through Rac1 and N-cadherin. *Stem Cells* **28**, 564–572 (2010).
- Yao, X., Peng, R. & Ding, J. Effects of aspect ratios of stem cells on lineage commitments with and without induction media. *Biomaterials* **34**, 930–939 (2013).
- Roman, J. & McDonald, J. A. Expression of fibronectin, the integrin alpha 5, and alpha-smooth muscle actin in heart and lung development. *Am. J. Respir. Cell Mol. Biol.* **6**, 472–480 (1992).
- Yang, Y., Relan, N. K., Przywara, D. A. & Schuger, L. Embryonic mesenchymal cells share the potential for smooth muscle differentiation: myogenesis is controlled by the cell's shape. *Development* **126**, 3027–3033 (1999).
- Tay, C. Y., Pal, M., Yu, H., Leong, W. S., Tan, N. S., Ng, K. W., Venkatraman, S., Boey, F., Leong, D. T. & Tan, L. P. Bio-inspired micropatterned platform to steer stem cell differentiation. *Small* **7**, 1416–1421 (2011).
- Rezakhaniha, R., Agianniotis, A., Schrauwen, J. T., Griffa, A., Sage, D., Bouten, C. V., van de Vosse, F. N., Unser, M. & Stergiopoulos, N. Experimental investigation of collagen waviness and orientation in the arterial adventitia using confocal laser scanning microscopy. *Biomech. Model. Mechanobiol.* **11**, 461–473 (2012).
- Bolte, S. & Cordelières, F. P. A guided tour into subcellular colocalization analysis in light microscopy. *J. Microsc.* **224**, 213–232 (2006).
- Tay, C. Y., Cai, P., Setyawati, M. I., Fang, W., Tan, L. P., Hong, C. H., Chen, X. & Leong, D. T. Nanoparticles strengthen intracellular tension and retard cellular migration. *Nano Lett.* **14**, 83–88 (2014).
- Rape, A. D., Guo, W. H. & Wang, Y. L. The regulation of traction force in relation to cell shape and focal adhesions. *Biomaterials* **32**, 2043–2051 (2011).
- Kurpinski, K., Lam, H., Chu, J., Wang, A., Kim, A., Tsay, E., Agrawal, S., Schaffer, D. V. & Li, S. Transforming growth factor-beta and notch signaling mediate stem cell differentiation into smooth muscle cells. *Stem Cells* **28**, 734–742 (2010).
- Clement, S., Stouffs, M., Bettli, E., Kampf, S., Krause, K. H., Chaponnier, C. & Jaconi, M. Expression and function of alpha-smooth muscle actin during embryonic-stem-cell-derived cardiomyocyte differentiation. *J. Cell Sci.* **120**, 229–238 (2007).
- Schildmeyer, L. A., Braun, R., Taffet, G., Debiasi, M., Burns, A. E., Bradley, A. & Schwartz, R. J. Impaired vascular contractility and blood pressure homeostasis in the smooth muscle alpha-actin null mouse. *FASEB J.* **14**, 2213–2220 (2000).
- McBeath, R., Pirone, D. M., Nelson, C. M., Bhadriraju, K. & Chen, C. S. Cell shape, cytoskeletal tension, and RhoA regulate stem cell lineage commitment. *Dev. Cell* **6**, 483–495 (2004).
- Young, D. A., Choi, Y. S., Engler, A. J. & Christman, K. L. Stimulation of adipogenesis of adult adipose-derived stem cells using substrates that mimic the stiffness of adipose tissue. *Biomaterials* **34**, 8581–8588 (2013).
- Sun, Y., Yong, K. M., Villa-Diaz, L. G., Zhang, X., Chen, W., Philson, R., Weng, S., Xu, H., Krebsbach, P. H. & Fu, J. Hippo/YAP-mediated rigidity-dependent motor neuron differentiation of human pluripotent stem cells. *Nat. Mater.* **13**, 599–604 (2014).
- Fu, J., Wang, Y. K., Yang, M. T., Desai, R. A., Yu, X., Liu, Z. & Chen, C. S. Mechanical regulation of cell function with geometrically modulated elastomeric substrates. *Nat. Methods* **7**, 733–736 (2010).
- Lam, C. R., Tan, C., Teo, Z., Tay, C. Y., Phua, T., Wu, Y. L., Cai, P. Q., Tan, L. P., Chen, X., Zhu, P. & Tan, N. S. Loss of TAK1 increases cell traction force in a ROS-dependent

- manner to drive epithelial-mesenchymal transition of cancer cells. *Cell Death Dis* **4**, e848 (2013).
- 31 Hinz, B., Celetta, G., Tomasek, J. J., Gabbiani, G. & Chaponnier, C. Alpha-smooth muscle actin expression upregulates fibroblast contractile activity. *Mol. Biol. Cell* **12**, 2730–2741 (2001).
- 32 Goffin, J. M., Pittet, P., Csucs, G., Lussi, J. W., Meister, J. J. & Hinz, B. Focal adhesion size controls tension-dependent recruitment of alpha-smooth muscle actin to stress fibers. *J. Cell Biol.* **172**, 259–268 (2006).
- 33 Hotulainen, P. & Lappalainen, P. Stress fibers are generated by two distinct actin assembly mechanisms in motile cells. *J. Cell Biol.* **173**, 383–394 (2006).
- 34 Vallenius, T. Actin stress fibre subtypes in mesenchymal-migrating cells. *Open Biol.* **3**, 130001 (2013).
- 35 Kovac, B., Teo, J. L., Makela, T. P. & Vallenius, T. Assembly of non-contractile dorsal stress fibers requires alpha-actinin-1 and Rac1 in migrating and spreading cells. *J. Cell Sci.* **126**, 263–273 (2013).
- 36 Vicente-Manzanares, M., Ma, X., Adelstein, R. S. & Horwitz, A. R. Non-muscle myosin II takes centre stage in cell adhesion and migration. *Nat. Rev. Mol. Cell Biol.* **10**, 778–790 (2009).
- 37 Tan, J. L., Ravid, S. & Spudich, J. A. Control of nonmuscle myosins by phosphorylation. *Annu. Rev. Biochem.* **61**, 721–759 (1992).
- 38 Mizutani, T., Haga, H., Koyama, Y., Takahashi, M. & Kawabata, K. Diphosphorylation of the myosin regulatory light chain enhances the tension acting on stress fibers in fibroblasts. *J. Cell Physiol.* **209**, 726–731 (2006).



This work is licensed under a Creative Commons Attribution 4.0 International License. The images or other third party material in this article are included in the article's Creative Commons license, unless indicated otherwise in the credit line; if the material is not included under the Creative Commons license, users will need to obtain permission from the license holder to reproduce the material. To view a copy of this license, visit <http://creativecommons.org/licenses/by/4.0/>

Supplementary Information accompanies the paper on the NPG Asia Materials website (<http://www.nature.com/am>)